

Evaluation Land Use -Land Cover Classification of Diyala River Area Using Landsat 8 Images

*Talal Hasan Kadhim

**Manal Shaker Al-kubaisi

* Ministry of Industry and Minerals / Iraqi Geological Survey

**University of Baghdad/ College of Science-Dept. of Geology

Baghdad-Iraq

E_mail: talalkazem@yahoo.com

Abstract

The land use-land cover map of the Diyala River basin was prepared based on the Landsat 8 satellite images that collected from 2018. The new classification procedures developed by the maximum likelihood probability method, with a field check being conducted between 2018 and 2019. Six major classes of the land use-land cover map were identified in the studied area: urban and built lands, forests, rangeland, agricultural lands, and water and barren lands. Each of the agricultural land class has been classified into three sub-class, which are cultivated land, harvested land, and cropland. While the barren land are classified into eight subclasses: slope sediments, conglomerates, carbonate rocks, sandstone rocks, clay rocks, loamy soil, exposed mixed rocks and mixed barren lands. The accuracy assessment for the land use-land cover map is 88.80 % and Kappa coefficient is 0.87.

Keywords: Diyala River, Landsat-8, Use-Land Cover, Maximum Likelihood Method, and Accuracy Assessment.

تقييم تصنيف استخدام الأرض - الغطاء الأرضي لمنطقة نهر ديالى باستخدام صور القمر

الصناعي لاندسات 8

طلال حسن كاظم * منال شاكر الكبيسي **

* وزارة الصناعة والمعادن / المسح الجيولوجي العراقي

** جامعة بغداد / كلية العلوم - قسم الجيولوجيا

بغداد - العراق

الخلاصة

تستخدم صور الأقمار الصناعية لإعداد خريطة استخدام الأراضي - الغطاء الأرضي (LULC) للمنطقة المدروسة اعتمادًا على صور القمر الصناعي Landsat8 OLI 2018 وإجراءات التصنيف التي تم تطويرها من قبل USGS، مع إجراء الفحص ميداني في عامي 2018 و2019. أنتجت خريطة استخدام الأراضي - الغطاء الأرضي اعتمادًا على طريقة الاحتمال القصوى (ML) لصور القمر لاندسات 8. تم تصنيف هذه الصور إلى ستة أصناف رئيسية واثني عشر صنف فرعي باستخدام برنامج ERDAS V. 2015 وتم تحويل صورة استخدام الأراضي - الغطاء الأرضي إلى بنية متجه باستخدام برنامج Arc GIS V. 10.2 من أجل إنشاء خريطة استخدام الأراضي - الغطاء الأرضي رقمياً. تم تحديد خمس أصناف رئيسية من خريطة استخدام الأراضي - الغطاء الأرضي في المنطقة المدروسة وهي: الأراضي الحضرية والمبينة، الغابات، المراعي، الأراضي الزراعية، المياه والأراضي القاحلة. وقسم كل من صنف الأراضي الزراعية إلى أربع أصناف فرعية وصنف الأراضي القاحلة إلى ثماني أصناف فرعية. وبلغت قيمة دقة التصنيف 88.80% ومعامل كابتا 0.87.

الكلمات المفتاحية: نهر ديالى ولاندسات8 واستخدام غطاء الارض وطريقة الاحتمالية العظمى وتقييم الدقة

Introduction

A supervised classification is widely used with a maximum likelihood algorithm to classify of the Landsat satellite Images (Lillesand, *et al.*, 2015). The different methods of supervised classification have been applied and experienced, extensively for land cover - land use (LCLU) management and planning for arid and semi-arid areas (Del Valle *et al.* 1998). LULC river basin mapping is a purposive tool that can be used for good management and planning of urbanization, agricultural applies and other human activities. The Landsat8 OLI satellite images data found to be suitable for the lithological units discrimination (Leverington and Moon 2012; Van der Meer, *et al.*, 1997), which shows a good spectral and spatial resolution for LULC analyses. Despite the importance of the Diyala River Basin (DRB), it is a little known about the LULC and it's affected on the planning and management for this basin. The maximum likelihood classifier (ML) is parametric and representing the most widely used classification technique (Foody, *et al.*, 1992; Hord 1982; Jensen, 2000). It assumes normal Gaussian distribution of multivariate data with pixels allocated to the most probable output LULC classes (Richards and Richards 1999). In several studies, MLC has been used effectively for classifying LULC and Other classes (Chen, *et al.*, 2004; Mishra, *et al.*, 2016; Mishra and Rai, 2016). Therefore, the effects of spatial resolution on LULC classification accuracy have received considerable attention due to the availability of a large variety of earth observation data.

The aim of this study concentrated on using landsat8 OLI sensor images to improve the LULC classification of the Diyala River Area by adding classes to the barren land class and accuracy assessment of classification by field.

Materials and Methods

Study Area

The DR area is a located between 44° 00' N to 48° 00' N longitudes and 33° 00' E to 36° 00' E latitudes and extends over an area of 26098 Km² (Figure 1). This area contains many LULC classes especially, the barren land class due to influence of stratigraphy, tectonic and structural in the study area.

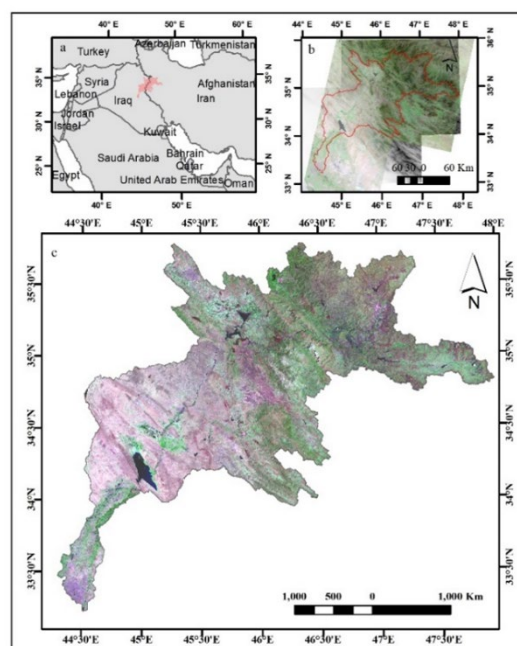


Figure (1) a) Location Map, b) Landsat Data (RGB753) with Hillshade and c) Landsat Image.

The Diyala River Basin is built up by different geological formations ranging in age from Triassic to recent as shown in Figure (2). The main stratigraphic sequence in the Diyala River Basin consists of Avroman limestone, Sarki, Sehkanyian, Sargelu, Naokedan Avannah, Pilaspi, Qulqula Series, Shiranish, Balambo, Tanjero Oligocene group, Euphrates-Jerebi, Fatha, Injana, Mukdadiyah, Bai Hassan, Bamu Conglomerate Formations and Quaternary deposits (Fouad and Sissakian 2015; Ghorbani 2013).

Materials

Five scenes from Landsat8 OLI (Viewer, 2012) were used in this study to perform LULC classification, with 30 m spatial resolution scenes acquired on 14 June 2018 and 21 June 2018 (Table 1).

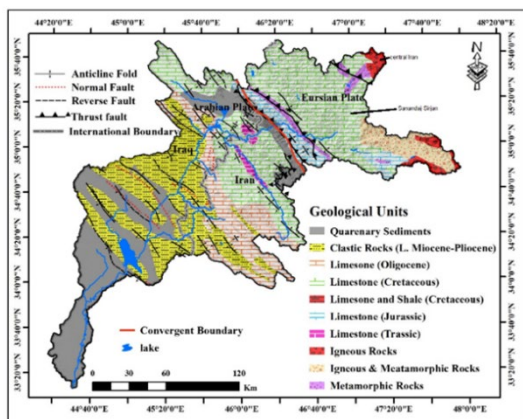


Figure (2) Geological Map of the Diyala River Basin (Fouad and Sissakian 2015; Ghorbani 2013).

Table (1) The Landsat8 OLI Scenes Used in this Study

Satellite: Landsat8	
Instrument: OLI	
Path / Row	Date
167/35	14/7/2017
167/36	14/7/2017
168/35	21/7/2017
168/36	21/7/2017
168/37	21/7/2017

Table (2) Landsat8 OLI Characteristics

B. No	B.N.	B. SR	B.GR
B1*	Coastal	0.43-0.45	30
B2	Blue	0.45-0.51	30
B3	Green	0.53-0.59	30
B4	Red	0.64-0.67	30
B5	NIR	0.85-0.88	30
B6	SWIR1	1.57-1.65	30
B7	SWIR2	2.11-2.29	30
B8*	Pano.	0.50-0.68	15
B9*	Cirrus	1.36-1.38	30
B10*	TIRS1	10.60-11.19	100
B11*	TIRS2	11.50-12.51	100

In addition, the ground truth information is combined with the help of high spatial resolution Quick Bird satellite images and Global Positioning System (GPS). The Landsat8 OLI dataset characteristics are shown in Table (2) Data and images in this study were processed in GIS (V10.2), ENVI (V.5.1) and ERDAS (V.2015) softwares.

Methods

Pre-Processing of Images

The first, the images are transformed from digital number to reflectance using the ENVI software. The second is performed the images layer stacking and mosaicking using ERDAS software. The layer stacking is used to create false-colour composite images as illustrated in Figure (1). The spatial analyst toolbox is used to extract the Diyala River Basin area by the subset by the mask tool in GIS software. It is important to implement geometric correction to produce a spatial distribution of LULC maps.

Class Signature Separability Analysis (CSSA)

The transformed divergence method (TD) is useful to separate the inter-classed signature analysis. The (TD) is a compute statistical distance between two class's signature (Training Samples). Besides, the (TD) is used for the separability evaluation between LULC classes before image classification. The TD values range from 0 to 2000 and represent how well the selected training samples are statistically distinguishable from each other. Generally, the (TD) value greater than is 1900 a good separability and the value less than 1700 a poor separability between two class's signature. The equation (1) used to conduct classes' separability analysis using the TD method for all datasets:

$$TD_{ij} = 2000[1 - \exp(-D_{ij}/8)] \dots \dots \dots (1)$$

TD_{ij}: the divergence between two classes signature, i and j: the two classes signatures being compared.

The Maximum Likelihood Probability

A maximum likelihood method (ML) was the common, widely used for supervised classification technique depended on the pixel likelihood belonging a specific class (Jensen, 2000). The (ML) is a parametric statistical approach that includes the normal class signatures distribution. The (ML) is a pixel-based technique depended on a multivariate probability density function for each class (Richards and Richards 1999). The (ML) technique uses class signatures (Training Samples) selected directly from the image to be determined the classes. The pixel belonging probability to one of the classes is calculated. Subsequently, a specific class is defined to the pixel with (ML). The equation (2) used to calculate ML:

$$D = \ln(a_c) - [0.5 \ln(|Cov_c|)] - [0.5(X - M_c)]^T (Cov_c^{-1}) (X - M_c) \dots\dots\dots (2)$$

D: weighted distance, c: particular class, X: vector candidate measurement pixel, M_c: mean vector of the sample of class, a_c: percent probability that any candidate pixel is a member of class, Cov_c: covariance matrix of the pixels in the sample of class, c: determinant of Cov_c, Cov_c⁻¹: inverse of Cov_c, ln: natural logarithm function and T: transposition function.

LULC classification Accuracy Assessment (CA)

The LULC classes are evaluated to check the validity and reliability of the produced LULC map. The LULC results are verified by calculating the user's accuracy (U_a), producer's accuracy (P_a), the overall accuracy (O_a), and Kappa coefficient (K_c) (Congalton 1991, 2001) It is not convenient to test every pixel of classified maps. Therefore, the test

samples (Reference Pixels Set) are combined with the help of field check. The (P_a), (U_a), (O_a), and (K_c) are calculated using equations as (3), (4), (5), and (6) respectively as follows:

$$U_a = \frac{n_{ii}}{n_{irow}} \dots\dots\dots (3)$$

$$P_a = \frac{n_{ii}}{n_{icol}} \dots\dots\dots (4)$$

$$O_a = \frac{(U_a + P_a)}{2} \dots\dots\dots (5)$$

$$K_c = N \sum_{i=1}^r n_{ii} - \sum_{i=1}^r \frac{n_{icol}n_{irow}}{N^2} - \sum_{i=1}^r n_{icol}n_{irow} \dots\dots\dots (6)$$

Results and Discussions

After deriving a set of spectral signatures, different decision rules can be used to classify each pixel from an image that covering the studied area. Fifteen classes were determined based on the spectral signature and the limited range between the minimum and the maximum values of the digital number that were displayed as average charts for each reflection class Figure (3). The (TD) values are calculated for all LULC classes' pairs in this study. The highest (TD) value is 2000. The (TD) values greater than 1900 is indicated better separability between two LULC classes. The detailed separability information analysis using (TD) for all the classes was shown in Table (3). After assembling training samples for each LULC class, Landsat8 OLI image classified using supervised ML. The classified image divided into six major LULC classes which urban-built up (1), water (2), forest (3), rangeland (5), agricultural land and barren land classes. The agricultural land class is divided into three subclasses they cropland and pasture (4), harvested (6), and cultivated (7) land. The barren land class divided into eight subclasses they mixed exposed rocks (8), conglomerates or/and (9)

loamy soil (10), carbonate rocks (11), sandstone (12), claystone (13), mixed barren land (14) and slope sediments (15) (Figure 4). The accuracy assessment result for ML based classified map of Landsat 8-OLI with 30m spatial resolutions in the Table (4). The (U_a), (P_a) and (O_a) values 88.49%, 89.71% and 88.8% respectively, with (K_c) value 0.87. The LULC class's area distribution are shown in Table (4). The (U_a) a

commission error measurement while (P_a) an omission error calculation for an individual LULC class. The classified image result indicated that (P_a) varied from 78% for sandstone subclass to 100% for built up. While (U_a) is varied from 70% for slope sediments subclass to 100% for cropland subclass.

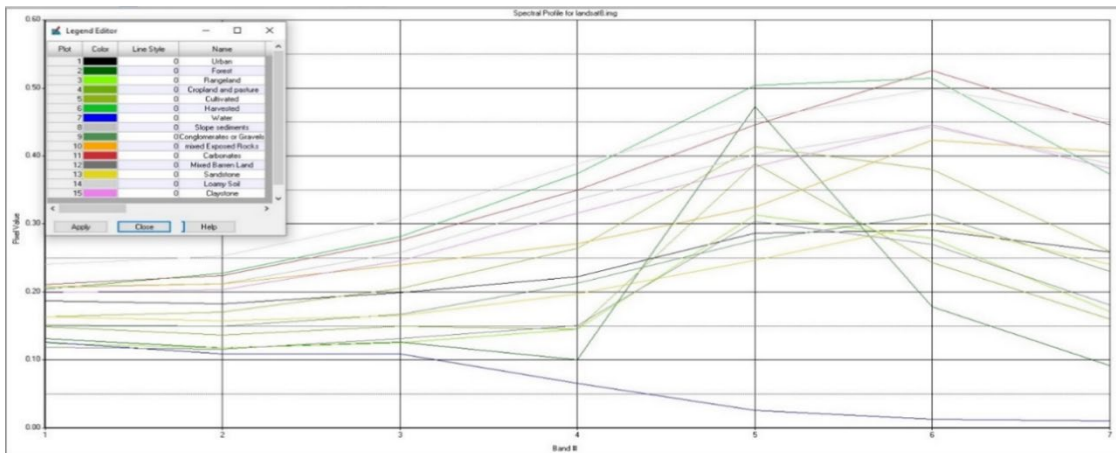


Figure (3) The Average Charts for Each Spectral Reflection Class

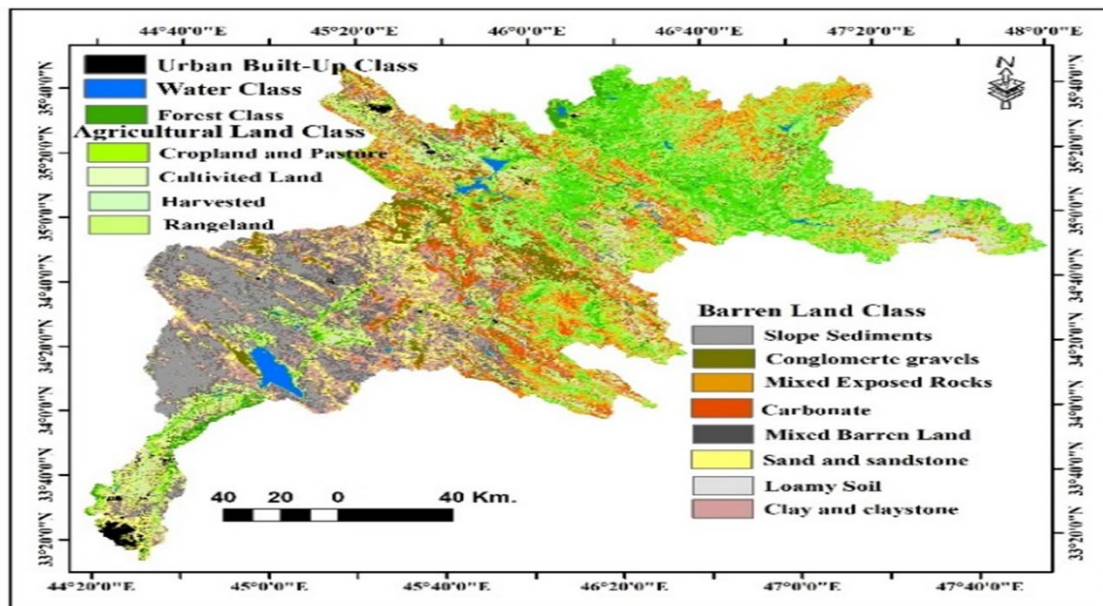


Figure (4) LULC Map of the DRB

Table (3) The (TD) Values between LULC Classes in the Study Area.

Class	1	2	3	4	5	6	7	8	9	10	11	12	13	14	15
1	x	2000	2000	2000	2000	2000	2000	2000	2000	2000	2000	2000	2000	2000	2000
2	2000	x	2000	2000	2000	2000	2000	2000	2000	2000	2000	2000	2000	2000	2000
3	2000	2000	x	2000	2000	2000	2000	2000	2000	2000	2000	2000	2000	2000	2000
4	2000	2000	2000	x	2000	2000	2000	2000	2000	2000	2000	2000	2000	2000	2000
5	2000	2000	2000	2000	x	2000	1999	2000	2000	2000	2000	2000	2000	2000	2000
6	2000	2000	2000	2000	2000	x	2000	2000	2000	2000	2000	2000	2000	2000	2000
7	2000	2000	2000	2000	1999	2000	x	2000	2000	2000	2000	2000	2000	2000	2000
8	2000	2000	2000	2000	2000	2000	2000	x	1999	2000	2000	2000	2000	2000	2000
9	2000	2000	2000	2000	2000	2000	2000	1999	x	2000	2000	2000	2000	2000	2000
10	2000	2000	2000	2000	2000	2000	2000	2000	2000	x	2000	2000	2000	2000	2000
11	2000	2000	2000	2000	2000	2000	2000	2000	2000	2000	x	2000	2000	2000	2000
12	2000	2000	2000	2000	2000	2000	2000	2000	2000	2000	2000	x	2000	2000	2000
13	2000	2000	2000	2000	2000	2000	2000	2000	2000	2000	2000	2000	x	2000	2000
14	2000	2000	2000	2000	2000	2000	2000	2000	2000	2000	2000	2000	2000	x	2000
15	2000	2000	2000	2000	2000	2000	2000	2000	2000	2000	2000	2000	2000	2000	x

Table (4) The P_a , U_a , K_c and O_a of the DRB.

Class	Ref.	C.T	No.Co.	$P_a\%$	$U_a\%$	K_c
1	25	30	25	100	83	0.82
2	26	31	25	96	81	0.80
3	41	34	33	80	97	0.97
4	42	37	37	88	100	1.00
5	29	33	28	97	85	0.84
6	37	35	35	95	100	1.00
7	32	34	31	97	91	0.91
8	30	33	28	93	85	0.84
9	42	35	35	83	100	1.00
10	31	34	29	94	85	0.84
11	26	33	23	88	70	0.68
12	40	34	31	78	91	0.90
13	36	33	30	83	91	0.90
14	37	33	30	81	91	0.90
15	26	31	24	92	77	0.76
To.	500	500	400			
Av. $O_a\%$				89.71	88.49 88.8	0.87

The results illustrated in Tables (4) and (5) indicated that there a larger difference in area calculations of forest and agricultural land. One explanation might be the contrasting classification between forest and agricultural land for multi-spectral satellite images. In addition, this study was restricted using level I and level II of Anderson classification (Anderson, *et al.*, 1976). The urban and builtup, forest, rangeland and water

classes restricted in level I. The agricultural land class restricted in level II and included the cropland, harvested and cultivated classes in level II. The barren land class was modified to suit the studied area that the slope sediments class added to level II and the exposed rocks class level II modified into five classes in level III, they are: claystone, sandstone, conglomerates, carbonates and mixed exposed rocks. The Barren

Land class level I a land of limited ability to support life and in which less than one-third of the area has vegetation or other cover (Kadhim, 2007). Generally, it is an area of thin soil, sand, or exposed rocks. The barren land class illustrated in Figure (4) within the studied area is involved into eight classes in level II and III. The Bare Exposed Rock, mixed barren land, and loamy soil classes in level II. In this study, the exposed rocks that belong to level II class is divided into four subclasses in level III they are claystone, sandstone, carbonates, and mixed exposed rocks. Depending on the spatial distribution of the reference points of the spectral signatures of the water class (form), there is no significant overlap with the spectral signatures of other classes. Due to the difference of the spectral signatures of water from other spectral signatures of other classes as shown in Figure (5).

In a few times observed, there is an overlap between the water class and the barren lands, especially when the water is very shallow which leads to its overlap with the barren lands. While the spectral signatures of both forests and agricultural lands (form) have resulted in an overlap between them, this may be the reason for this overlap, as they contain close proportions of the chlorophyll at times. To resolve of these overlaps, the QuickBird satellite image is used to illustrate the interaction between water and loamy soil as shown in Figure (5) which illustrates the overlap between forests and agricultural land as shown in Figure (6). In addition, the fieldwork checking is used to resolve these overlaps (Figure 6). The surface cover database identified in the study area through the landsat8 data, maximum likelihood method classification Figure (6) provides surface cover data generally consistent with ground-truth information and enhances the information presented with geological maps.

Table (5) The Classes Area of the DRB

Class Name	Level No	Area km ²	Area %
Urban	I	422	1.28
Water	I	430	1.31
Forest	I	980	2.98
Cropland	II	1548	4.82
Pasture	II	3384	10.29
Cultivated	II	4924	14.98
Harvested	II	1440	4.38
Mixed Exposed Rocks	III	3552	10.81
Conglomerate	III	2257	6.87
Loamy or Bare Soil	II	2099	6.39
Carbonate	III	2236	6.80
Sandstone and Sand	III	2091	6.36
Claystone and Clay	III	3073	9.35
Mixed Barren Land	II	2462	7.49
Slope Sediments	II	1937	5.89
Total		32871	100

Class pairs that have been successfully discriminated in the classified database include (1) slope sediments (Fine-clastic Rock Fragments) from Tanjero, Plasipi, Fatha, Injana, Mukdadiyah, Bai Hassan and the erosion deposits from other Formations in the area, (2) mixed exposed rock (Igneous or /and Metamorphic Rocks), (3) Conglomerates (or /and Gravel) from Bai Hassan and Bamu Formations and less amounts from the river terraces, (4) carbonate rocks (Limestone and Dolomite) from Avroman limestone, Sarki, Sehkanyian, Sargelu, Naokedan Avanah, Pilaspi, Qulqula Series, Shiranish, Balambo,

Tanjero Oligocene group, Euphrates-Jerebi Formations, (5) sandstone from Fatha Injana and Mukdadiyah formations, (6) claystone (or/ and siltstone) from Fatha Injana and Mukdadiyah formations, (7) loamy soil (silty clayey soil) from residual soil and (8) mixed barren land from mixed of barren land and agricultural classes. Similarly, claystone and sandstone are relatively well discriminated in the database.

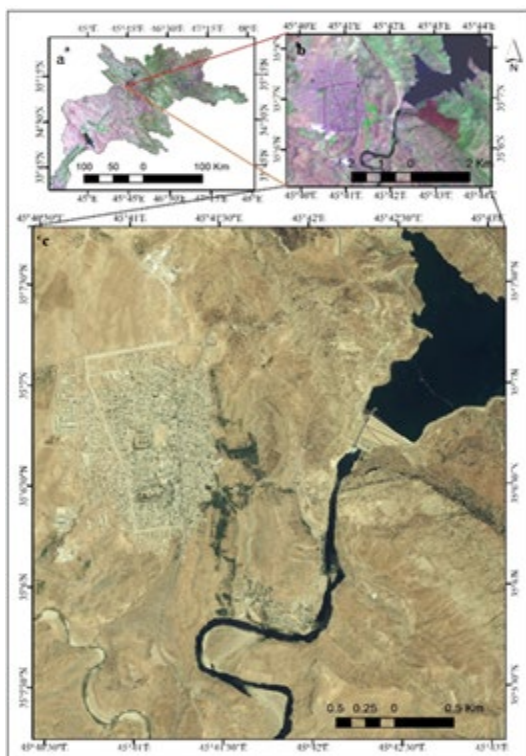


Figure (5), (a,b) The Landsat8 Image of Derbandikhan Lake and c) The Quickbird Image of Derbandikhan Dam.



Figure (6) Carbonate Rocks, Range-land and Mixed Barren Land Classes in The Studied Area

Though vegetation cover class exposed was properly defined in unmixed results, the expected exposure of eight key lithological subclasses wasn't really fully consistent with ground truth. The fraction image for the mixed exposed rock subclass was appropriately highlights the general surface distribution of this subclass, but it does not properly depict smaller outcrops of igneous or/and metamorphic rocks and was incorrectly predicts low to moderate exposure of this subclass over much of the study area. Because of its exposures covered by plants, the most area that inside Iranian territory, it was not checked in the field. The limited benefit of not mixing the results in this study indicates the needed to enhance the spectral resolution of the input image data, which can increase the number of permissible final units and can also help with the spectral separation of the lithological subclasses of importance (Leverington and Moon 2012; Van Der Meer and de Jong 2001). The results were collected from this study highlighting both the significant benefit with the Landsat8 image and the limitations observed in the lithological classes in the study area. In general, the ML classification methods for each pixel in landsat8 image based distinction of lithological groups with properties similar to these in subclasses and associated units was much greater benefit than other techniques due to their dependence on the assumes normal distribution of the histogram of the data bands, which it is a mean the ML classification method based on the spectral and spatial distribution of the cell's (pixel) digital number (Hord 1982; Van der Meer, *et al.* 1997). Ambiguity between the mixed exposed rock and the loamy bare soil subclasses of is more difficult, but it is essentially limited to areas of substantial plant that is covered

in the study area toward to the northeast part.

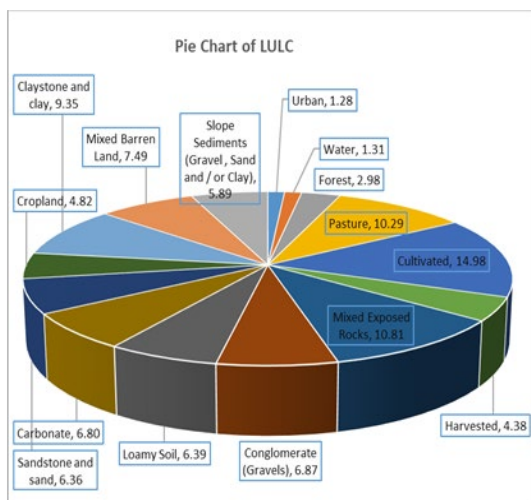


Figure (7) Pie Chart of LULC Area and Percentage

Besides looking at the spectral limitations of landsat8 images, the ML classification and linear no-mixing procedures that used in this study may have been undermined by the partial lichen cover of exposed materials in the study area. The effects of lichen complexity are well known for the multi-spectral and super-spectral action involving the northern, northeastern and eastern study parts (Rollin, *et al.*, 1994) and in non-mixing exercises it can ideally be best mitigated by defining separate end-lichen end organs for example, (Rogge, *et al.* 2007). As mentioned above, it is also likely that the mixing procedures have become more complicated due to the spectral diversity of the lithological classes in the study area. However, the ML of pass forward back propagation can efficiently parameterize variance in the spectral characterization of training data (Leverington, 2001). The un-mixing technique basically assumes spectral uniformity inside individual interest classes. The overall accuracy assessment (O_a) of the classified map Figure (4) reaches 88.8%, which is very good value (Congalton 1991, 2001), with the

exception of the carbonate subclass reached a precision of 79% (P_a equal to 88% and U_a equal to 70%), because it is the most carbonate rock exposures covered by a thin soil layer, and its have the vertical or oblique exposures, which affects the spectral signatures of these rocks, for more details see table (4). The identified fifteen classes of the LULC classes in the studied area that acquired from the (ML) have various distributions in the Table (5) and Figure (7).

Conclusions

The LULC area was measured in km² and percentage for each class in the studied area. The barren land class is the prevalent in the study area, which has an area of about 22694 km² and a percentage of about 69%. The slope sediments class has a large coverage area is 4924 km² and the percentage about 14.98% in the DRB area. The data reveal that the barren land class includes the mixed exposed rocks and the mixed barren land. The mixed exposed rocks class is involved the igneous and/or metamorphic rocks with the other rocks has a coverage area 3552 km² with percentage about 10.81% in the DRB. The other classes' area range from 980 to 3384 km² and percentage range from 2.89% to 10.29% Table (5). The agricultural land class includes cultivated, harvested and croplands which represents the secondary class in the studied area. Forest Land is represented the third class in the studied area. While the water and urban classes are the smallest area within the studied area, which is about 422 km² (1.28%), and 430 km² (1.31%), respectively Table (5). Therefore, six main classes of LULC have noted in the studied area, these are urban and built-up land, forest, rangeland, agricultural land, water and barren land classes. The most common class within the studied area are the barren land class area and the agricultural

land class that occurs in the most parts of the studied.

References

- Anderson**, B. J. R.; Hardy, E. E.; Roach, J. T., and Witmer, R. E. (1976). A Land Use and Land Cover Classification System for Use with Remote Sensor Data. U.S. Geological Survey Professional Paper 964 (Vol. 2001).
- Chen**, D., Stow, D. A. and Gong, P. (2004). Examining the Effect of Spatial Resolution and Texture Window Size on Classification Accuracy: An Urban Environment Case. *International Journal of Remote Sensing* 25(11), 2177–2192.
- Congalton**, R. G. (1991). A Review of Assessing the Accuracy of Classifications of Remotely Sensed Data. *Remote Sensing of Environment*, 37(1), 35–46.
- Congalton**, R. G. (2001). Accuracy Assessment and Validation of Remotely Sensed and Other Spatial Information. *International Journal of Wildland Fire*, 10(4), 321–328.
- Del Valle**, H. F.; Elissalde, N. O.; Gagliardini, D. A., and Milovich, J. (1998). Status of Desertification in the Patagonian Region: Assessment and Mapping from Satellite Imagery. *Arid Land Research and Management*, 12(2), 95–121.
- Foody**, G. M.; Campbell, N. A.; Trodd, N. M., and Wood, T. F. (1992). Derivation and Applications of Probabilistic Measures of Class Membership from the Maximum-Likelihood Classification. *Photogrammetric Engineering and Remote Sensing*, 58(9), 1335–1341.
- Fouad**, S. F. A., and Sissakian, V. K. (2015). Geological Map of Iraq, Scale 1: 1000 000, 2012. *Iraqi Bulletin of Geology and Mining*, 11(1), 9–16.
- Ghorbani**, M. (2013). A Summary of Geology of Iran. *The Economic Geology of Iran* pp. 45–64. Springer.
- Hord**, R. M. (1982). *Digital Image Processing of Remotely Sensed Data*. Elsevier.
- Jensen**, J. R. (2000). *Remote Sensing of the Environment: An Earth Resource Perspective*. Prentice-Hall.
- Kadhim**, T. (2007). Series Of Land Use - Land Cover Maps OF Iraq Scale 1:250 000 Khanaqin Quadrangle Sheet No. NI - 38 - 7 (LULCM 15).
- Leverington**, D. W. (2001). Discriminating Lithology in Arctic Environments from Earth Orbit an Evaluation of Satellite Imagery and Classification Algorithms.
- Leverington**, David W., and Moon, W. M. (2012). Landsat-tm-based Discrimination of Lithological Units Associated with the Purtuniqu Ophiolite, Quebec, Canada. *Remote Sensing*, 4(12), 1208–1231.
<https://doi.org/10.3390/rs4051208>
- Lillesand**, T., Kiefer, R. W., and Chipman, J. (2015). *Remote Sensing and Image Interpretation*. John Wiley and Sons.
- Mishra**, V. N., Rai, P. K., Kumar, P., and Prasad, R. (2016). “Evaluation of Land Use/Land Cover Classification Accuracy Using Multi-Resolution Remote Sensing Images.” *Forum Geografic XV* (1), 45–53.
- Mishra**, V. N., and Rai, P. K. 2016. A Remote Sensing Aided Multi-layer Perceptron-markov Chain Analysis for Land Use and Land Cover Change Prediction in Patna District (Bihar), India. *Arabian Journal of Geosciences* 9(4), 249.
- Richards**, J. A., and Richards, J. A. (1999). *Remote Sensing Digital Image Analysis* (Vol. 3). Springer.
- Rogge**, D. M., Rivard, B., Zhang, J., Sanchez, A., Harris, J., and Feng, J.

(2007). Integration of Spatial-spectral Information for the Improved Extraction of Endmembers. *Remote Sensing of Environment*, 110(3), 287–303.

Rollin, E. M.; Milton, E. J., and Roche, P. (1994). The Influence of Weathering and Lichen Cover on the Reflectance Spectra of Granitic Rocks. *Remote Sensing of Environment*, 50(2), 194–199.

Van Der Meer, F.; Vazquez-torres, M., and Van Dijk, P. M. (1997). Spectral Characterization of Ophiolite Lithologies in the Troodos Ophiolite Complex of Cyprus and Its Potential in Prospecting for Massive Sulphide Deposits. *International Journal of Remote Sensing*, 18(6), 1245–1257.

Van Der Meer, Freek, and de Jong, S. M. (2001). *Imaging Spectrometry Basic Principles and Prospective Applications (Vol. 1)* [BOOK]. Springer Science and Business Media.

Viewer, U. G. V. (2012). URL: <http://glovis.USGS.gov>. Accessed 20th April.